

# Particle transport and flow modification in planar temporally evolving laminar mixing layers. I. Particle transport under one-way coupling

Chidambaram Narayanan<sup>a)</sup> and Djamel Lakehal<sup>b)</sup>

*Institute of Energy Technology, Swiss Federal Institute of Technology, ETH-Zentrum/CLT, CH-8092 Zurich, Switzerland*

(Received 1 December 2005; accepted 31 July 2006; published online 14 September 2006)

Simulations of two-dimensional, particle-laden mixing layers were performed for particles with Stokes numbers of 0.3, 0.6, 1, and 2 under the assumption of one-way coupling using the Eulerian-Lagrangian method; two-way coupling is addressed in Part II. Analysis of interphase momentum transfer was performed in the Eulerian frame of reference by looking at the balance of fluid-phase mean momentum, mean kinetic energy, modal kinetic energy, and particle-phase mean momentum. The differences in the dominant mechanisms of vertical transport of streamwise momentum between the fluid and particle phases is clearly brought out. In the fluid phase, growth of the mixing layer is due to energy transfer from the mean flow to the unstable Kelvin-Helmholtz modes, and transport of mean momentum by these modes. In contrast, in the particle phase, the primary mechanism of vertical transport of streamwise momentum is convection due to the mean vertical velocity induced by the centrifuging of particles by the spanwise Kelvin-Helmholtz vortices. Although the drag force and the particle-phase modal stress play an important role in the early stages of the evolution of the mixing layer, their role is shown to decrease during the pairing process. After pairing, the particle-phase mean streamwise momentum balance is accounted for by the convection and drag force term. The particle-phase modal stress term is shown to be strongly connected to the fluid phase modal stress with a Stokes-number-dependent time lag in its evolution. © 2006 American Institute of Physics. [DOI: [10.1063/1.2352728](https://doi.org/10.1063/1.2352728)]

## I. INTRODUCTION

Interest in particle/droplet flows is prompted by their importance to many industrial processes such as atomization, spray-injection systems, powdered-fuel combustion, particle separators, and in the environmental sciences such as sedimentation phenomena, pollutant transport in the atmosphere, etc. Importance of large-scale flow structures in particle dispersion and transport is now fully recognized.<sup>1</sup> Large-scale structures are responsible for particles concentrating in certain regions of the flow, which in turn affects the flow strongly in these regions. In many practical applications, mixing layers represent a unit configuration controlling cross-stream transport of mass, momentum, and energy. Study of particle dispersion, accumulation, and flow modulation by particles in mixing layers is, therefore, challenging and has potential for wide applicability.

The study of particle-laden or dispersed-phase flow can be split into two components (not necessarily independent). One part is the study of particle transport due to the underlying fluid flow, such that the presence of particles does not affect the flow or *one-way* coupling. Particles, due to their inertia, do not follow the path of a fluid element that starts at the same position at a given time. The goal of such studies is to predict particle dispersion, transport, or accumulation in selective regions of the flow, based on the knowledge of the flow field. For one-way coupling to be a valid assumption,

particle volume fractions and mass fractions should be much less than one. However, for particles much denser than the carrier fluid, such as in gas-solid flows, a small volume fraction can result in a mass fraction of the order of one. In this case, the presence of particles can significantly alter the flow evolution, although particle-particle interactions could still be neglected. Such a situation is referred to as *two-way* coupling. A more detailed description of the different regimes of particulate flows has been presented by Elghobashi.<sup>2</sup>

The study of the growth of a mixing layer has been a long-time endeavor of fluid dynamicists over the last several decades.<sup>3-7</sup> A laminar mixing layer is unconditionally unstable to perturbations and it grows due to unstable streamwise modes. This instability, known as the Kelvin-Helmholtz (KH) instability, can be understood by a classical linear stability analysis including the effect of particles.<sup>8,9</sup> As the instability modes grow, the most unstable mode or the fundamental mode dominates the growth of the mixing layer, resulting in the formation of prominent spanwise KH vortices.

After the formation of KH vortices, several possibilities exist for the further evolution of a mixing layer: Under strong spanwise forcing, the rolled up mixing layer is susceptible to spanwise instabilities, which results in three-dimensionalization.<sup>10,11</sup> On the other hand, if the subharmonic mode is strongly forced, pairing of two neighboring vortices can occur wherein three-dimensionalization is suppressed or delayed. The subharmonic velocity field induces two spanwise vortices to turn around each other and merge, to form one large vortex. In essence, the mixing layer

<sup>a)</sup>Electronic mail: [chidu@iet.mavt.ethz.ch](mailto:chidu@iet.mavt.ethz.ch)

<sup>b)</sup>Author to whom correspondence should be addressed. Electronic mail: [lakehal@iet.mavt.ethz.ch](mailto:lakehal@iet.mavt.ethz.ch)

is sensitive to external forcing (conditions at the splitter plate) and retains memory of this for a long time.

In practice, both the above possibilities, viz., three-dimensionalization and pairing, coexist, and the mixing layer eventually turns turbulent. In the seminal work of Roshko and co-workers,<sup>6,12</sup> which refocused the attention of turbulence research on coherent structures in turbulence, it was shown that vortical structures related to the initial instability persist even after the flow becomes turbulent. The turbulent mixing layer is thus a combination of organized wave motion (the KH vortex and its subharmonic) upon which broadband turbulent fluctuations are superimposed. However, by keeping the spanwise extent of the flow domain small in a simulation, the spanwise instabilities can be suppressed and the flow remains planar. Such a situation provides the opportunity to isolate the effects of the organized motion on particle transport, and vice versa.

### Studies on particle dispersion (one-way coupling)

One of the first experiments on particle-laden mixing layers was performed by Lazaro and Lasheras.<sup>13</sup> Their preliminary investigations were furthered in a series of papers by Lasheras *et al.*<sup>14–17</sup> They noticed that the response of the particles to the coherent velocity field consisting of the KH vortices, leads to a selective dispersion of droplets along the mixing layer, with a higher concentration of smaller droplets in the core of the vortices. Later experiments<sup>14</sup> report the existence of large-scale particle streaks emanating from the undisturbed spray. They also report the presence of two layers flanking the vortex cores, where local accumulation of larger particulates occurs. For forced mixing layers, they<sup>15</sup> observed a higher degree of activity and coherency in the particle concentration field.

Hishida *et al.*<sup>18</sup> present measurements of particle and gas velocities and particle number densities for a turbulent mixing layer with glass particles. They found that the particle fluctuating velocity approaches that of the gas phase with decreasing particle size and increasing width of the mixing layer. Experiments by Wen *et al.*<sup>19</sup> also reinforce the dominant effect of the large-scale vortices in particle dispersion.

Experiments typically study the dispersion of particles in *spatially* evolving mixing layers. In such experiments the velocity ratios (ratio of the velocity difference to the mean velocity) are of the order of 1, and hence the experiments cannot be directly compared to a temporally evolving mixing layer. With the exception of Ref. 17, the above experiments have considered *one-way* coupling situations. A range of particle Stokes numbers have been studied for both natural and forced mixing layers with laminar and turbulent inflow conditions. Basic effects such as the accumulation of particles in the outer region of the Kelvin-Helmholtz vortices and the effect of pairing in homogenizing the particle distribution have been observed. Some detailed results on the kinetic energy transfer between the phases and particle-induced dissipation have been reported.<sup>16,17</sup>

There have been many numerical studies of particle dispersion in mixing layers with one-way coupling. One of the early studies on the effect of vortex pairing on particle dis-

persion was performed by Chein and Chung.<sup>20</sup> They show using Lagrangian statistics that particles with small Stokes numbers disperse laterally at approximately the same rate as fluid particles and that particles with large Stokes numbers disperse much less than the fluid particles. Particles with intermediate Stokes numbers (0.5–5) may disperse more than the fluid particles, because they are unable to exactly follow the rotational motion induced by the vortices. They also showed that the pairing process produces higher particle lateral dispersion than the pre- and post-pairing flows.

A series of studies on the accumulation and dispersion of heavy particles in forced two-dimensional mixing layers has been carried out by Meiburg and collaborators. Martin and Meiburg<sup>21</sup> drew attention to the formation of highly concentrated particle streaks in the braid region between two vortices. This work was extended by Raju and Meiburg<sup>22</sup> by considering the effect of gravitational settling. Marcu and Meiburg<sup>23–25</sup> used an analytical model for the stretched counter rotating streamwise vortices that appear in three-dimensional mixing layers<sup>26</sup> to isolate the effect of these vortices on particle accumulation. Equilibrium points for the particles and their stability were determined analytically, accounting also for gravity. They found that in the absence of gravity, accumulation of moderate-Stokes-number particles can occur only at the center of the braid vortices.

Aggarwal *et al.*<sup>27</sup> presented numerical simulation results for spatially developing mixing layers with particles. They showed that particles injected into the faster stream exhibited higher dispersion compared to those injected in the slower stream, which was attributed to the asymmetric entrainment in a mixing layer. Hu *et al.*<sup>28</sup> also presented results on particle dispersion in spatially evolving mixing layers. They note in particular that the effects of neighboring vortex structures on particle transport cannot be accounted for in a temporal simulation. Wang *et al.*<sup>29</sup> focused on the idea of non-uniform seeding of particles to maximize lateral particle dispersion in two-dimensional mixing layers. They showed that nonuniform seeding can significantly enhance the dispersion of particles but the location maximizing lateral dispersion is both time and Stokes number dependent.

Soteriou and Yang<sup>30</sup> investigated the dispersion of particles in a spatially evolving mixing layer between two streams of different velocity, density, and viscosity. They found that variations in the viscosity ratio did not significantly alter the relationship between Stokes number and dispersion, however, it did result in reduced dispersion for higher viscosity ratios. With respect to variations in density, maximum dispersion was found to be for the uniform density case for particles with intermediate Stokes numbers. They showed that the mechanism of baroclinic vorticity generation played an important role in creating asymmetry in particle dispersion. Recently, Yang *et al.*<sup>31</sup> studied particle dispersion using a discrete vortex model approach. Their conclusions are in accordance with previous studies about the Stokes number dependence of dispersion.

Earlier studies have not clarified all the issues, and many interesting questions remain to be answered. The controlling mechanisms for the growth of the particle-phase mixing layer have not been analyzed in detail. The magnitude of the

mean particle-phase vertical velocity induced by the KH vortices as a function of particle Stokes number is a key unknown quantity. Some of the other questions addressed by this study are: How is the particle-phase modal stress correlated to the fluid phase modal stress? and, What is the relative importance of the particle-phase modal velocity field in driving particle-phase mixing layer growth?

The present study analyses in detail the particle-laden mixing layer problem: the first part deals with mechanisms of particle transport in two-dimensional mixing layers and the second part analyses the impact of particles on its growth and evolution. Particle transport in a forced planar mixing layer is simulated using an Eulerian-Lagrangian method. However, instead of focusing on Lagrangian dispersion indicators as in previous work, this study focuses on particle transport in an Eulerian frame and identifies the dominant mechanisms of momentum and energy transport in both phases. To set the stage for the analysis of the impact of particles on the mechanisms underlying mixing layer growth, the mean and modal kinetic energy balances are analyzed in detail.

The presentation structure is as follows. The upcoming section details the governing equations and the numerical method used. Results are presented in two parts: the first part characterizes the growth of the mixing layer using various indicators such as average modal stress and mean kinetic energy balance. The second part, discusses the motion of particles of different Stokes numbers under one-way coupling. The important transport mechanisms for the particle-phase momentum are elucidated by looking at the streamwise momentum balance.

## II. GOVERNING EQUATIONS AND NUMERICAL METHOD

A Lagrangian particle-tracking module<sup>32</sup> was developed and coupled with an incompressible Navier-Stokes solver. The following equation for the particle motion in a dilute suspension of small, rigid, and heavy particles under Stokes-flow conditions was used:<sup>33</sup>

$$\frac{d\mathbf{u}_p}{dt} = -f_D \frac{9\mu}{2\rho_p a^2} \{\mathbf{u}_p - \mathbf{u}[\mathbf{x}_p(t)]\}, \quad (1)$$

where  $\mathbf{u}_p(u_p, v_p, w_p)$  is the velocity of a particle,  $\mathbf{x}_p$  is its position,  $\mathbf{u}(u, v, w)$  is the velocity of the fluid interpolated onto the particle position,  $\rho_p$  is the particle density,  $\mu$  is the fluid viscosity,  $a$  is the particle radius, and  $f_D$  is given by

$$f_D = 1 + 0.15\text{Re}_p^{2/3}. \quad (2)$$

The continuous phase is represented by the incompressible Navier-Stokes equations given by

$$\frac{\partial u_j}{\partial x_j} = 0 \quad (3)$$

and

$$\frac{\partial u_i}{\partial t} + u_j \frac{\partial u_i}{\partial x_j} = -\frac{1}{\rho_f} \frac{\partial p}{\partial x_i} + \frac{1}{\text{Re}} \frac{\partial^2 u_i}{\partial x_j^2} + F_i^{fp}, \quad (4)$$

where  $F_i^{fp}$  is the fluid-particle interaction force per unit mass. The coupling between the fluid and the particles is achieved by projecting the force acting on each particle onto the flow grid. The fluid-particle interaction force vector  $\mathbf{F}^{fp}$  has the following form at a grid node  $\mathbf{x}^m$ :

$$\mathbf{F}_m^{fp} = \sum_{\alpha=1}^{N_p} \frac{\rho_p V_p}{\rho_f V_m} R_{rc} \mathbf{f}^\alpha W(\mathbf{x}^\alpha, \mathbf{x}^m), \quad (5)$$

where  $\alpha$  stands for the particle index,  $N_p$  for the total number of particles in the flow,  $\mathbf{f}^\alpha$  for the force on a single particle centered at  $\mathbf{x}^\alpha$  [given by Eq. (1)],  $R_{rc}$  for the ratio between the actual number of particles in the flow and the number of computational particles, and  $W$  for the projection weight of the force on to the grid node  $\mathbf{x}^m$ , which is calculated based on the distance of the particle from those nodes to which the particle force is attributed.  $V_m$  is the fluid volume surrounding each grid node, and  $V_p$  is the volume of a single particle.

The velocity interpolation (onto particle position) method was tested in an earlier study.<sup>32</sup> Fourth-order-accurate Lagrangian polynomial interpolation was found to be adequate for this class of problems. The particle equation was integrated using a second-order Runge-Kutta method that gave results identical to those of a fourth-order version.

The Navier-Stokes solver uses a pseudo-spectral collocation method, employing Fourier modes in the streamwise and spanwise directions and Chebyshev polynomials in the vertical, nonperiodic direction. The solver is specially designed to simulate a temporally evolving mixing layer where the vertical dimension, infinite in extent, is mapped onto a  $[-1, 1]$  domain using an exponential mapping function. Further details of the numerical procedure can be found in Cortesi *et al.*<sup>11</sup>

## III. TWO-DIMENSIONAL MIXING LAYER: BASIC FLOW FEATURES

A two-dimensional mixing layer was simulated for a Reynolds number,  $\text{Re}=400$ , defined based on the initial vorticity half-thickness and the velocity half-difference. The domain size in the streamwise direction was set to  $4\pi/k_r$ , where  $k_r=0.4418$  is the most unstable wavenumber obtained from linear stability analysis. The vertical extent of the domain is infinity, which is made possible by resorting to an appropriate coordinate transformation.<sup>11</sup> The domain was discretized using 64 Fourier collocation points in the streamwise direction and 129 Chebyshev collocation points in the vertical direction.

The flow was initialized using a hyperbolic-tangent mean streamwise velocity profile to which perturbations were added.<sup>34</sup> The initial amplitudes of fundamental and the subharmonic modes were chosen such that the whole simulation period included the saturation of the fundamental mode and vortex nutation, followed by the increase in the energy of the subharmonic mode which results in the pairing of the two KH vortices. The initial perturbation amplitudes

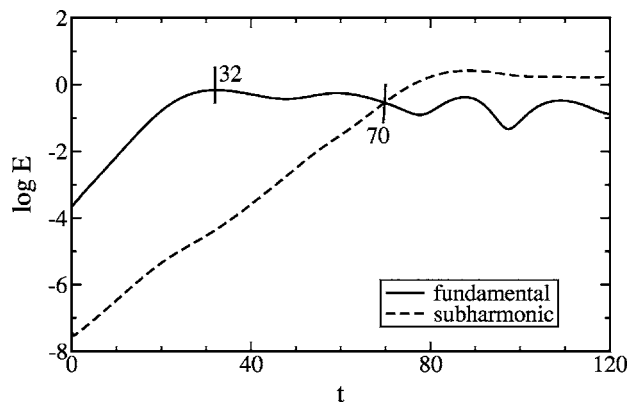


FIG. 1. Evolution of the fundamental and subharmonic mode energies.

were  $\epsilon_f=10^{-2}$  and  $\epsilon_s=10^{-4}$ , where the subscripts  $f$  and  $s$  denote the fundamental and subharmonic modes, respectively.

The evolution of the kinetic energy in the fundamental and subharmonic modes is shown in Fig. 1. The fundamental mode is seen to saturate at a nondimensional time of 32, after which the energy in the mode oscillates until the subharmonic mode gains significant energy. We define the point of intersection between the two energies as a time marking the beginning of the pairing process. The pairing process results in a significant increase in the mixing layer thickness and can be assumed to have ended at  $t \approx 90$ , when the energy in the subharmonic mode reaches a maximum.

Snapshots of spanwise vorticity at different time instants are shown in Fig. 2. The following conditions of the flow can

be observed: saturated fundamental mode undergoing vortex nutation at  $t=48$ , initiation of pairing at  $t=72$ , ending of the pairing process at  $t=96$ , and a single large vortex at  $t=120$ .

The evolution of the mean kinetic energy, the modal kinetic energy, and the total kinetic energy within a fixed domain size in the vertical direction ( $-50 \leq z \leq 50$ ) is shown in Fig. 3(a) (mean and modal velocity and kinetic energy are defined in Secs. III A and III B, respectively). In order to visualize the mean and modal energies in the same plot the initial total kinetic energy is added to the modal kinetic energy. The quantities are then normalized by the total initial kinetic energy. Thus, Fig. 3(a) actually shows the *total*, *mean*, and *modal+total* kinetic energies. One can clearly see the exchange of energy between the mean and the wave components. The modal energy shows a first peak at around  $t=32$  and then oscillates until the start of pairing. After this peak there is a reverse flow of energy from the modes to the mean, as seen from Fig. 3(a), where a reduction in the modal energy results in an increase in the mean energy. This oscillation in the modal energy is called *vortex nutation*.<sup>35</sup> This phenomenon is in contrast to broadband turbulence, where the net flow of energy is from the larger to the smaller scales. The presence of organized motion makes this aspect of energy transfer important.

As will be shown in Sec. III B, the transfer of energy from the mean to the modes is given by  $-\langle u'w' \rangle d\langle u \rangle/dz$ , where  $\langle \rangle$  denotes an average along horizontal  $x$ - $y$  planes ( $\langle u_i \rangle$  denotes the mean and  $u'_i$  the modal velocity). Therefore, the direction of energy flow is controlled by the sign of  $-\langle u'w' \rangle$  as  $d\langle u \rangle/dz$  is always positive in this flow.  $-\langle u'w' \rangle$  is

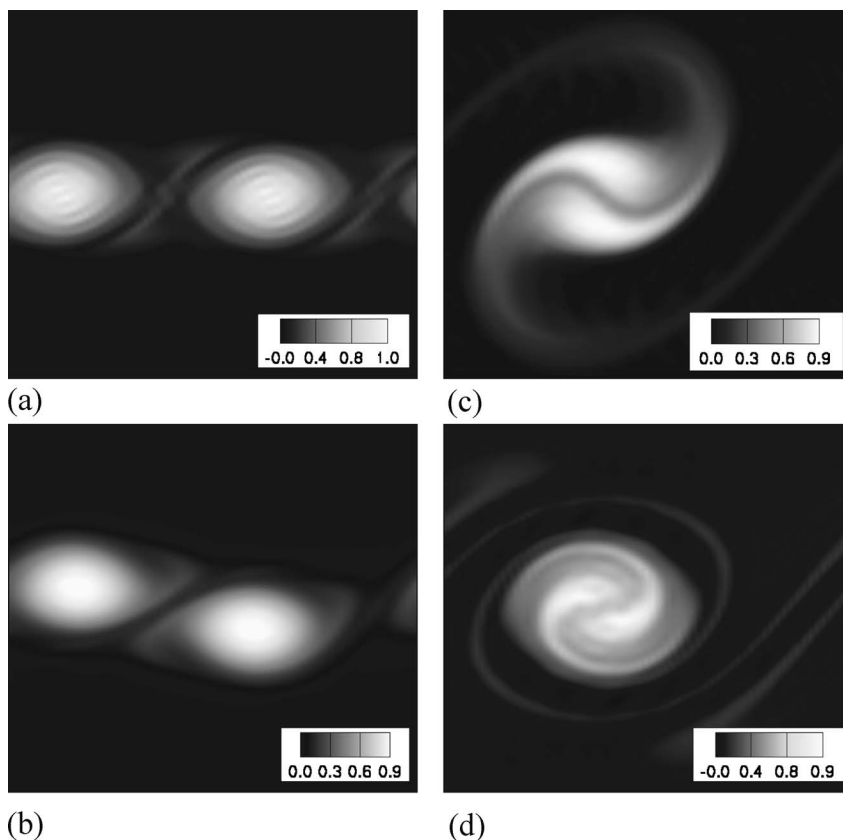


FIG. 2. Spanwise vorticity contours for a particle-free mixing layer at different time instants. (a)  $t=48$ —nutation; (b)  $t=72$ —pairing initiation; (c)  $t=96$ —pairing; (d)  $t=120$ —post pairing.

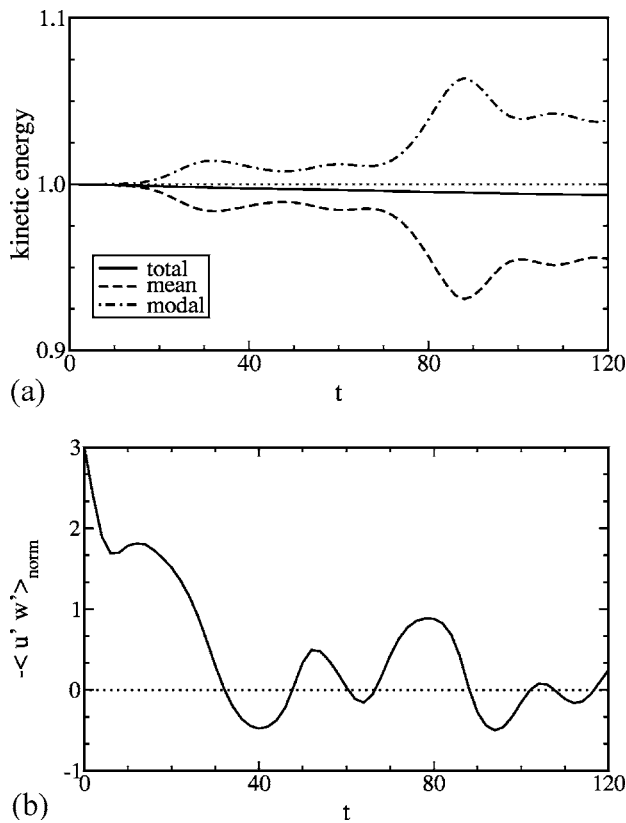


FIG. 3. Evolution of (a) total kinetic energy, mean kinetic energy, and modal kinetic energy, and (b) modal stress averaged over the vertical direction.

the *modal stress* arising due to the spatial averaging of the organized waves. Figure 3(b) shows the evolution of the modal stress (normalized by  $u'_{\text{rms}}$  and  $w'_{\text{rms}}$ ) with time, where a single number at every time has been obtained by further averaging along the vertical direction.

A positive value for the modal stress denotes a transfer of energy from the mean flow to the modes and vice versa. The modal stress changes sign at  $t=32$ , which is the point of maximum energy in the fundamental mode. The change in sign of the modal stress implies a lack of self similarity for mixing layers that are strongly forced at the most unstable frequencies; the mixing layer does not grow linearly with time, instead, it has periods of growth interspersed with periods of shrinkage. This behavior has also been observed in experiments on force mixing layers.<sup>36</sup> The oscillation in the average modal stress after  $t=32$  denotes vortex nutation, whereby the fundamental mode exchanges energy with the mean until the subharmonic mode gains in energy. The zero-crossing of the average modal stress at  $t \approx 90$  denotes the point of maximum energy in the subharmonic mode followed by nutation of the large vortex after pairing. The pairing process results in a large transfer of energy from the mean to the waves.

### A. Mean momentum balance for the fluid phase

Throughout this study, the Eulerian viewpoint in describing the flow has been preferred over Lagrangian statistics. As a first step, we look at the balance equations for the mean momentum of the fluid phase in this section. Splitting the

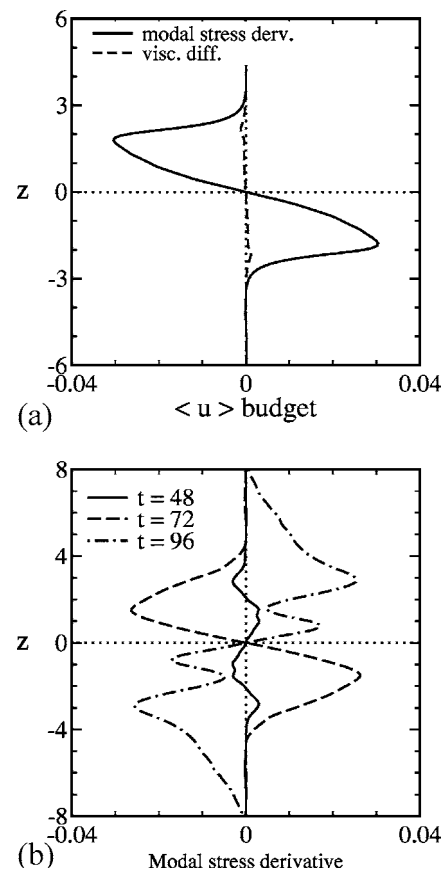


FIG. 4. Profiles of the viscous diffusion and modal stress derivative terms in the mean streamwise momentum balance equation. (a)  $t=24$ ; (b) modal stress derivative.

instantaneous streamwise fluid velocity  $u(x, z, t)$  into the mean  $[\langle u \rangle(z, t)]$  and modal  $[u'(x, z, t)]$  components by averaging the Navier-Stokes equations along the streamwise direction, we obtain the nondimensional balance equation for the mean streamwise velocity  $\langle u \rangle$ :

$$\frac{\partial \langle u \rangle}{\partial t} = -\frac{\partial \langle u'w' \rangle}{\partial z} + \frac{1}{\text{Re}} \frac{\partial^2 \langle u \rangle}{\partial z^2} + \langle f_{x,CD} \rangle, \quad (6)$$

where  $f_{x,CD}$  denotes the total interaction force per unit mass between the particle and the fluid phases. The balance for the mean vertical velocity is obtained as

$$-\frac{\partial \langle w'w' \rangle}{\partial z} = \frac{\partial \langle p \rangle}{\partial z} + \langle f_{z,CD} \rangle, \quad (7)$$

because the mean vertical velocity  $\langle w \rangle$  always remains zero by virtue of continuity. The mean momentum balance in the vertical direction will not be presented as it is not dynamically significant. The terms arising due to the presence of particles and two-way coupling are introduced here for use in Part II.

The two terms in the right-hand side (RHS) of Eq. (6) at  $t=24$  are presented in Fig. 4(a). At  $t=0$ , the viscous term is larger than the modal stress derivative  $[-\partial \langle u'w' \rangle / \partial z]$ , because the initial amplitudes of the perturbations are very small; however, at  $t=24$ , the viscous term is negligible as compared to the modal stress derivative term. As expected,

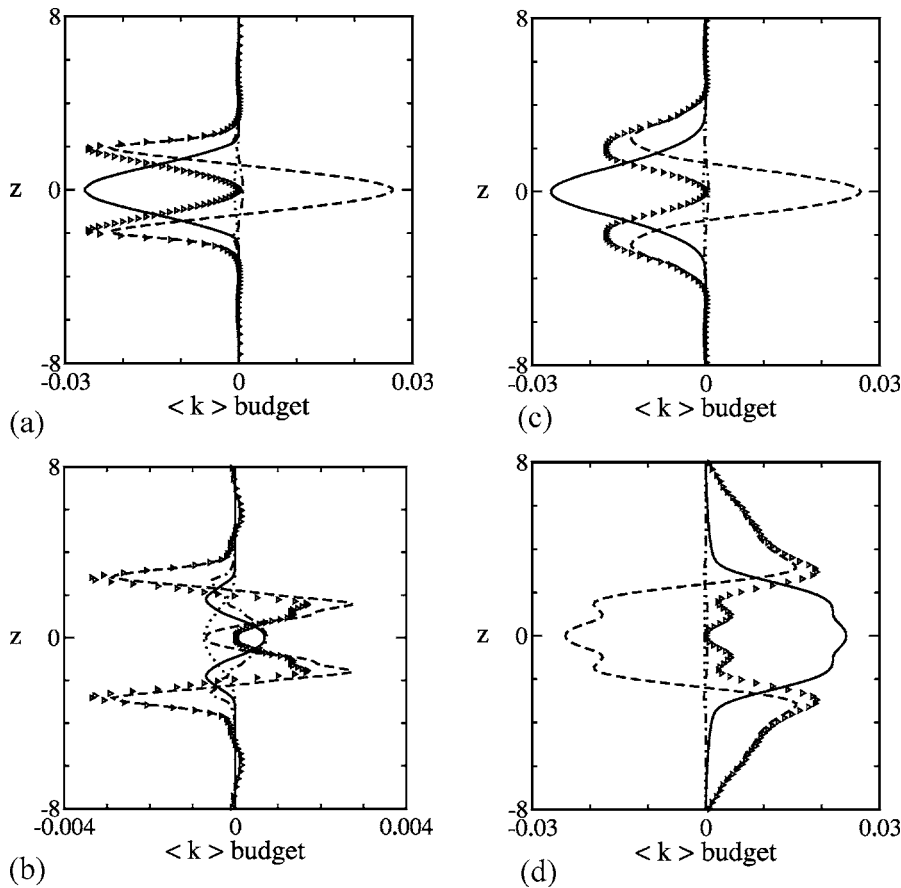


FIG. 5. The mean kinetic energy balance at different time instants. Legend: (---) viscous diffusion; (···) viscous dissipation; (—) energy exchange term; (- · -) transport by the modes; (▷▷▷) sum of the RHS. (a)  $t=24$ ; (b)  $t=48$ ; (c)  $t=72$ ; (d)  $t=96$ .

the value of the modal stress derivative is positive in the lower part of the domain, where it increases the mean velocity, and negative in the upper region, where it decreases the mean velocity. The modal stress derivative is the main agent of evolution of the mean streamwise velocity.

The modal stress derivative profiles at selected times are presented in Fig. 4(b). From Fig. 3(b), we see that around  $t=48$  the mixing layer is not growing much due to fundamental mode saturation. This implies a small value for the modal stress derivative term. At  $t=72$  the mixing layer is poised to grow rapidly due to incipient pairing, and at  $t=96$  the mixing layer is shrinking and hence the sign at this time instant is reversed.

**B. Kinetic energy balances**

Using the mean and modal fluid velocities  $\langle u_i \rangle$  and  $u'_i$ , respectively, the balance of the mean kinetic energy  $\langle k \rangle = 1/2 \langle u_i \rangle \langle u_i \rangle$  is given as follows:

$$\frac{\partial \langle k \rangle}{\partial t} = \underbrace{\frac{1}{\text{Re}} \frac{\partial^2 \langle k \rangle}{\partial z^2}}_{(I)} - \underbrace{\frac{1}{\text{Re}} \left( \frac{\partial \langle u \rangle}{\partial z} \right)^2}_{\text{modal transp. (II)}} - \underbrace{\frac{\partial}{\partial z} (\langle u \rangle \langle u' w' \rangle)}_{\text{modal transp. (II)}} + \underbrace{\langle u' w' \rangle \frac{\partial \langle u \rangle}{\partial z}}_{\text{exchange (III)}} + \underbrace{\langle u \rangle \langle f_{x,CD} \rangle}_{\text{force term (IV)}} \tag{8}$$

where the first two and the fourth terms in the RHS are the viscous diffusion, viscous dissipation, and the energy ex-

change between the mean and the modes, respectively (modes include all finite length scales in the flow; however, most of the energy is accounted for by the fundamental and the subharmonic modes). The third term is the conservative transport of mean kinetic energy by the modes and the last term is the energy exchange between the particles and the fluid. In Eq. (8), the most important term governing the dynamics of the mixing layer is the energy exchange term (it also appears in the modal kinetic energy equation).

The balance of the average modal kinetic energy  $\langle k' \rangle = 1/2 \langle u'_i u'_i \rangle$  is given as follows:

$$\frac{\partial \langle k' \rangle}{\partial t} = \frac{1}{\text{Re}} \frac{\partial^2 \langle k' \rangle}{\partial z^2} - \frac{1}{\text{Re}} \left\langle \left( \frac{\partial u'_i}{\partial x_j} \right)^2 \right\rangle - \underbrace{\langle u' w' \rangle \frac{\partial \langle u \rangle}{\partial z}}_{\text{exchange (II)}} - \underbrace{\frac{1}{2} \frac{\partial}{\partial z} (\langle u' u' w' \rangle + \langle w' w' w' \rangle)}_{\text{modal diff. (III)}} - \underbrace{\frac{\partial}{\partial z} \langle p' w' \rangle}_{\text{pres. diff. (IV)}} + \underbrace{\langle u' f'_{x,CD} \rangle + \langle w' f'_{z,CD} \rangle}_{\text{force term (V)}} \tag{9}$$

where the index notation is used only for the second term in the RHS. The terms in the RHS are viscous diffusion, viscous dissipation, energy exchange with the mean, transport by the modes, pressure diffusion, and fluid-particle interaction terms.

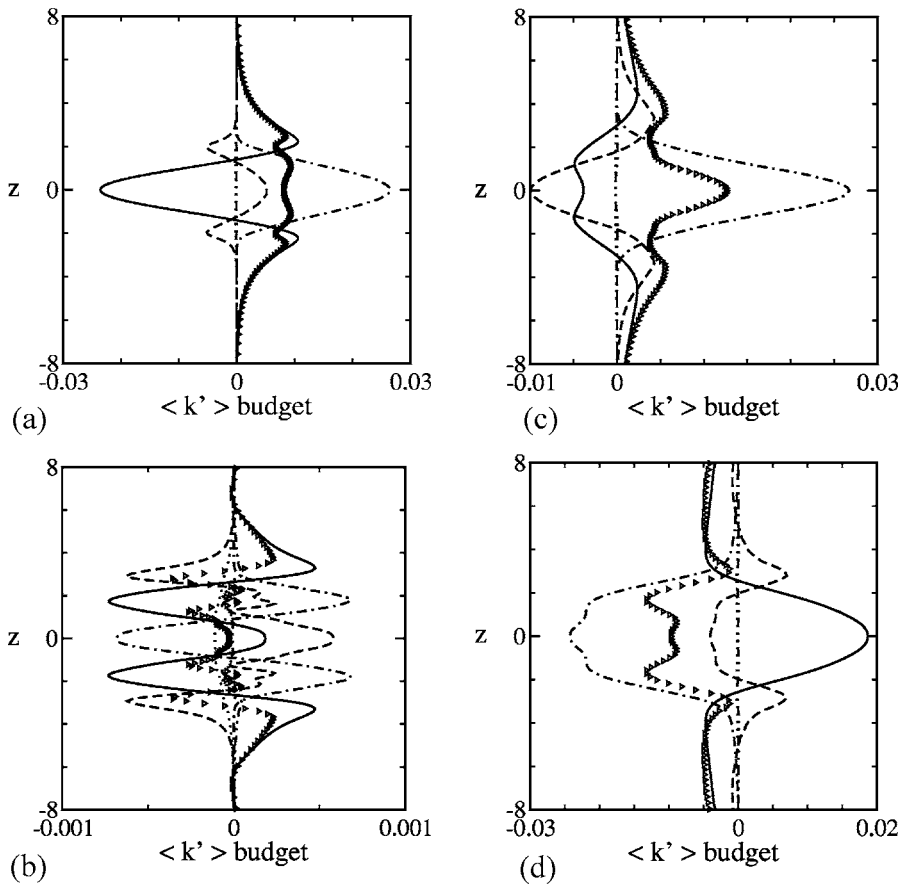


FIG. 6. The modal kinetic energy balance at different time instants. Legend: (---) viscous diffusion; (····) viscous dissipation; (- - -) energy exchange term; (- - -) transport by the instability modes; (—) pressure diffusion; (▷▷▷) sum of the RHS. (a)  $t=24$ ; (b)  $t=48$ ; (c)  $t=72$ ; (d)  $t=96$ .

The mean kinetic energy balance at different time instants is shown in Fig. 5. As can be expected for a laminar free-shear flow at moderate to high Reynolds numbers, the viscous diffusion and dissipation terms are much smaller than all the other terms, except at  $t=48$ . At this time, the fundamental mode is saturated and the mixing layer is not growing anymore; due to this, all the other terms are more than one order of magnitude smaller compared to other times. Note that the sign of the energy exchange term is not uniform at this time, which means that at this time, there is no net exchange of energy between the mean and the modes, but local exchanges are ongoing. At  $t=24$  and  $72$ , the mixing layer is growing and the energy transfer term is strongly negative. In contrast, at  $t=96$ , the mixing layer is shrinking and the energy transfer term is positive (transfer of kinetic energy from the modes to the mean). For a growing mixing layer  $\partial\langle k \rangle / \partial t$  is negative and vice versa. The other significant term in the mean kinetic energy balance is the transport term due to the modes. This represents the effect of the modal velocity field in transporting (diffusion in turbulence parlance) mean kinetic energy. Therefore, the dynamics of a mixing layer can be closely understood by analyzing the mean kinetic energy balance, also in the case of particle-fluid interaction.

The modal kinetic energy balance at different time instants is shown in Fig. 6. Here, too, depending on the time instant at which the mixing layer is growing or shrinking, the net balance of all the terms in the RHS of Eq. (9) is positive ( $t=24, 72$ ) or negative ( $t=96$ ). Except at  $t=48$ , the viscous

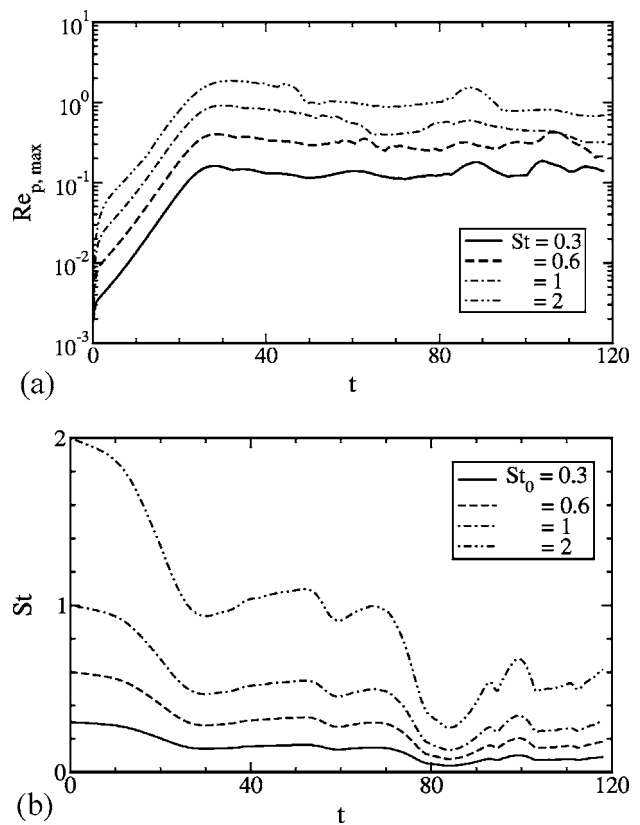


FIG. 7. Variation of (a) the maximum particle Reynolds number and (b) the effective Stokes number, with time for different Stokes numbers.

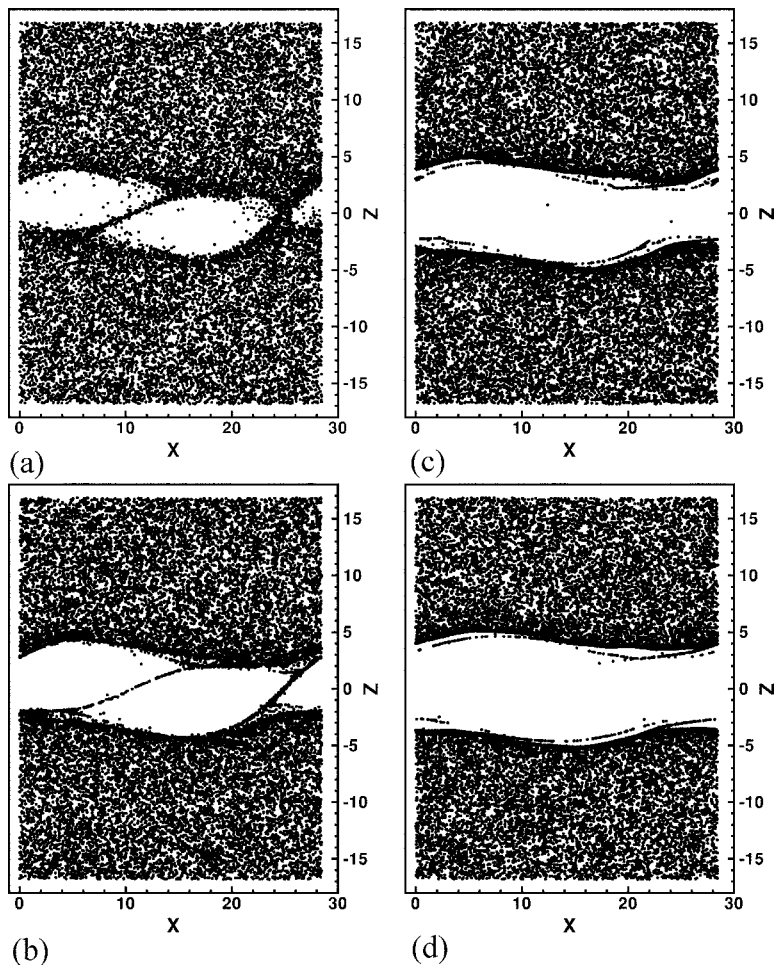


FIG. 8. Particle patterns in a vertical plane at  $t=72$ . (a)  $St=0.3$ ; (b)  $St=0.6$ ; (c)  $St=1$ ; (d)  $St=2$ .

diffusion and dissipation terms are negligible compared to the energy exchange, pressure diffusion, and transport by the modes. All the transport terms become smaller in magnitude at  $t=48$  where the mixing layer is at almost zero growth stage. It is interesting to note the oscillatory behavior of the terms. As compared to the  $\langle k \rangle$  equation, an additional term in the form of the pressure diffusion exists in the modal kinetic energy equation. This term, along with the transport by the modes, acts as a conservative distribution agent (these terms are usually called diffusion terms in turbulence parlance but in the absence of small scales they retain their convective character here). The main idea behind presenting the above balances is to contrast this with the particle-phase balances and also analyze the effect of particles, under the assumption of two-way coupling, to these transport mechanisms; this latter analysis will be presented in Part II of the study.

#### IV. PARTICLE TRANSPORT UNDER ONE-WAY COUPLING

In this section, results from the simulations of particle-laden mixing layers under the assumption of one-way coupling are presented. The same calculation as the particle-free flow was recalculated with four particle Stokes numbers: 0.3, 0.6, 1, and 2. As an initial condition, the particles were randomly distributed in the domain with their velocities set

equal to the fluid velocity at their positions. Particle data were stored every two nondimensional time units.

The particles were tracked in a three-dimensional domain obtained by adding spanwise planes to the two-dimensional fluid computational domain. The two-dimensional flow velocity was then copied on to these extra planes. This was required by the interpolation algorithm for calculating the flow velocity at particle positions (four spanwise planes for a fourth-order method). Particle statistics, for example number density, were calculated by first averaging in the spanwise direction and then in the streamwise direction ( $x$ ). For each Stokes number, 100 000 particles were tracked.

Throughout the period of the simulation, the average particle Reynolds number  $Re_p$  was significantly smaller than 1 for all cases. The maximum particle Reynolds number was less than 2 at all times. Figure 7(a) shows the evolution of the maximum particle Reynolds number with time. However, the values of the maximum particle Reynolds numbers show the correction to the Stokes drag to be small.

Before proceeding further with the analysis, it is important to mention that as the mixing layer grows in time, the mean flow time scale increases. Since the ratio between the initial vorticity half-thickness and the velocity half-difference is used as the reference time scale to define the Stokes numbers mentioned above, effectively, the particle

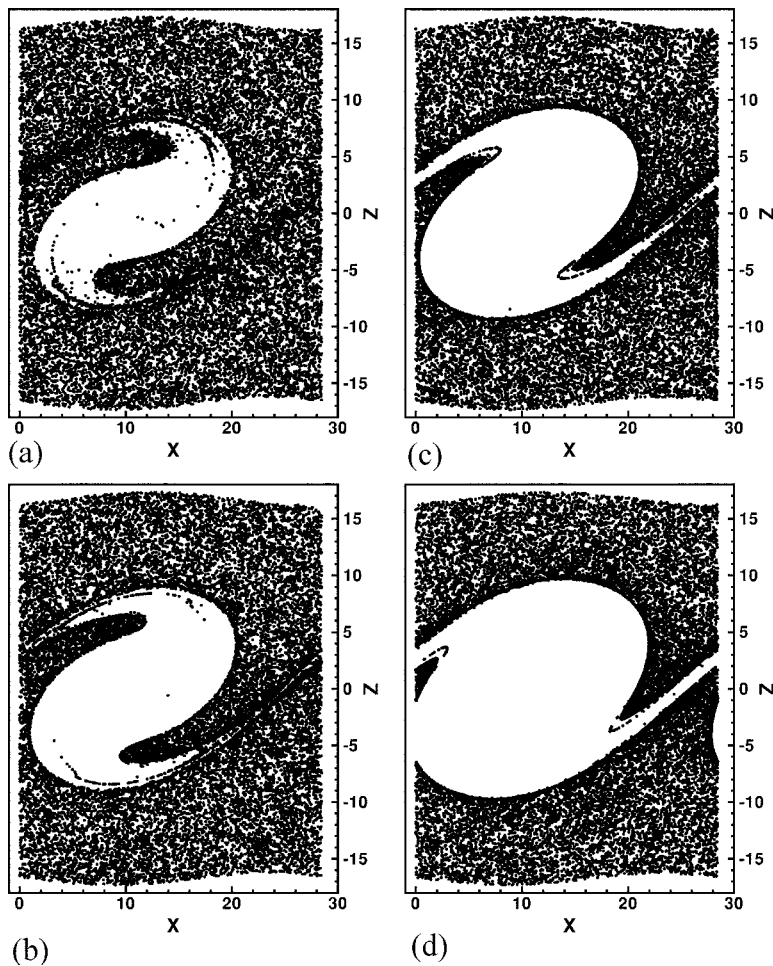


FIG. 9. Particle patterns in a vertical plane at  $t=96$ . (a)  $St=0.3$ ; (b)  $St=0.6$ ; (c)  $St=1$ ; (d)  $St=2$ .

response to the flow becomes faster with time. This is because the vorticity half-thickness increases with time, whereas the velocity difference remains constant, implying an increasing fluid flow time scale. To illustrate this, the evolution of the *effective* Stokes number given as  $St_{t=0} \delta_{\omega h}(0) / \delta_{\omega h}(t)$  is shown in Fig. 7(b). It can be anticipated that such a reduction in the effective Stokes number must result in a reduction in the particle Reynolds numbers with time, which can be gleaned from Fig. 7(a). In addition, from Fig. 7(b) we see that particles with  $St=2$  can be expected to participate in the pairing process the most, because at the time of pairing initiation they have an effective Stokes number of approximately one; as known from previous studies, particles with Stokes number of unity respond the most to the flow.<sup>20</sup>

### A. Centrifuging effect

It is a known fact<sup>20</sup> that as the KH vortices develop, particles start to move towards the edges of the vortices. For the range of Stokes numbers considered, the higher Stokes number particles leave the vortex cores faster and accumulate more in the periphery and in the braid region connecting the two vortices. The best way to observe this is to look at snapshots of the particle positions at different times. In the following sequence of figures (Figs. 8 and 9), particle

patterns for all the four Stokes numbers are shown at  $t=72$  and 96.

The evacuation of the central part of the domain proceeds at a rapid pace for  $St=1$  and 2, such that at  $t=72$  (Fig. 8) the whole region is devoid of particles. However, the pairing process (Fig. 9) re-entrains a large number of particles back into the central region, specifically at the braid region. After the pairing, a situation similar to the pre-pairing time repeats because the only remaining braid region now again has accumulated particles just as before. This is significant especially for  $St=1$  and 2 particles, because before pairing the whole central region was devoid of particles. An important characteristic of mixing layer evolution is the sustained presence and influence of the KH vortices. In contrast to turbulent flows, where a degree of randomness prevents formation of persistent patterns, the action of the KH vortices for a long period of time results in selective accumulation of even small Stokes number particles.

The total number of particles at any time in the central section of the mixing layer  $z \in (-2, 2)$  for all the Stokes numbers is shown in Fig. 10. Clearly the depletion rate is much higher for larger Stokes numbers. Surprisingly, the total number of particles coming back to the central section during the pairing process is greater than the initial number.

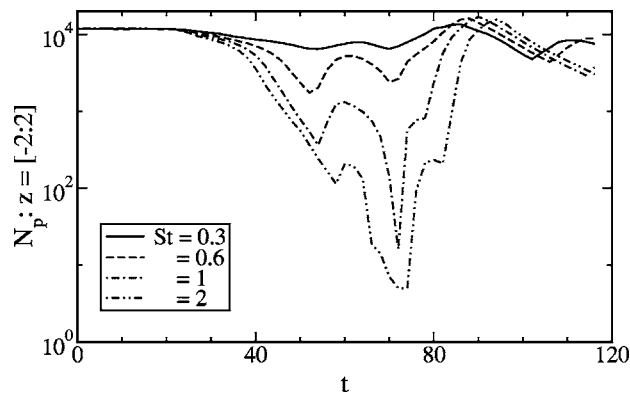


FIG. 10. Number of particles in the region  $z \in (-2, 2)$ .

The rate of depletion directly implies the presence of a mean particle vertical velocity (the fluid has a zero mean vertical velocity).

### B. Particle statistics

Studies on particle dispersion in turbulent flows have revealed the phenomenon of preferential accumulation of particles.<sup>1,37</sup> It is well established that inertial particles will migrate away from circulating regions and accumulate in streaming and stagnation zones. The accumulation of particles and the patterns formed thereof depend on the inertia of the particle, the time scale and intensity of structures in the flow and for this particular case also on the *lifetime* of the

KH vortices. In two-dimensional mixing layers, preferential concentration occurs mainly due to the sustained churning effect of the KH vortices, which then undergo an organized pairing process. The folding event results in thin regions of high particle concentration sandwiched between regions devoid of particles.

We look now at horizontal-plane ( $x$ - $y$ ) averaged particle statistics. Local Eulerian quantities such as number density  $n$  and particle velocity  $u_{pi}$  are calculated by averaging in a volume around the computational node, which are then averaged over the horizontal plane. The profiles for the number density and other quantities shown below have been smoothed to make them presentable as otherwise they would be noisy. Smoother average quantities can be obtained by increasing the number of particles tracked;<sup>38</sup> however, since the motivation is to analyze the relative importance of different transport mechanisms such an attempt was not made. A simple discrete smoothing function using a three-point stencil was used, and five iterations were carried out. Figure 11 shows the number density profiles, normalized by the initial uniform number density value, at different times. The primary effect of preferential accumulation in two-dimensional mixing layers is evident. The accumulation at the periphery is significant, especially for larger Stokes numbers. At  $t=96$ , after the pairing has taken place, multiple peaks in the number density profiles are visible, which signify alternate bands with and without particles. Due to the streamwise average, the tendency of particles to accumulate in the braid region is not clearly brought out in these profiles.

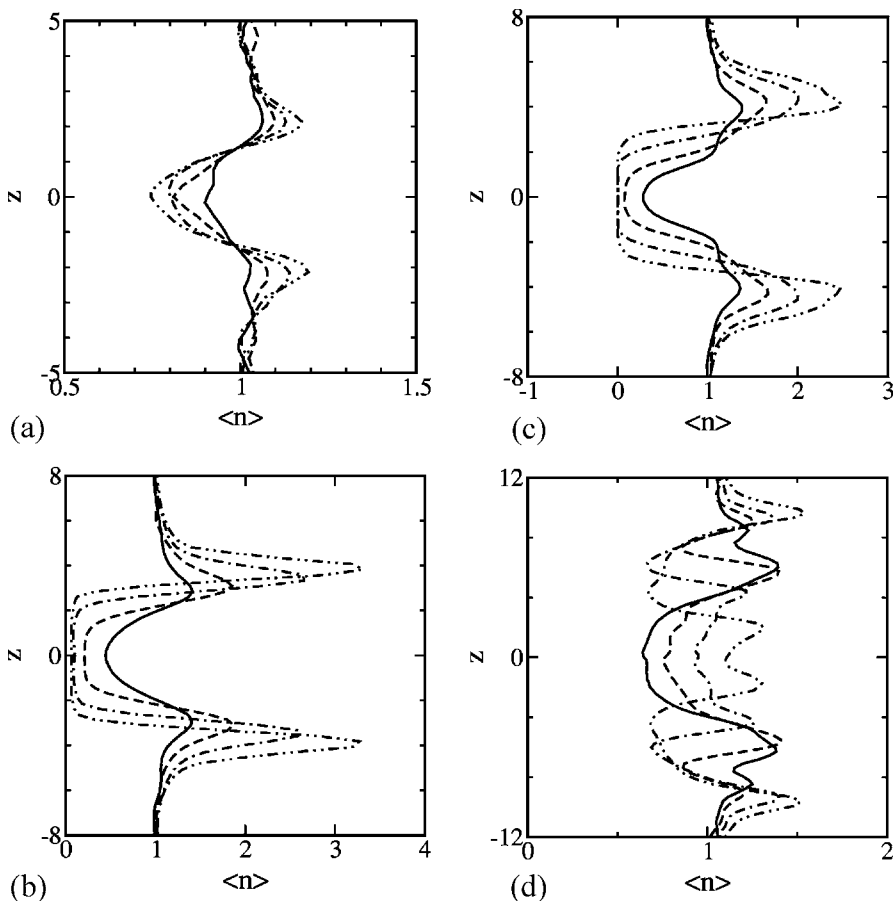


FIG. 11. Particle number density profiles for different Stokes numbers. Legend: (—)  $St=0.3$ ; (- - -)  $St=0.6$ ; (- · -)  $St=1$ ; (· · ·)  $St=2$ . (a)  $t=24$ ; (b)  $t=48$ ; (c)  $t=72$ ; (d)  $t=96$ .

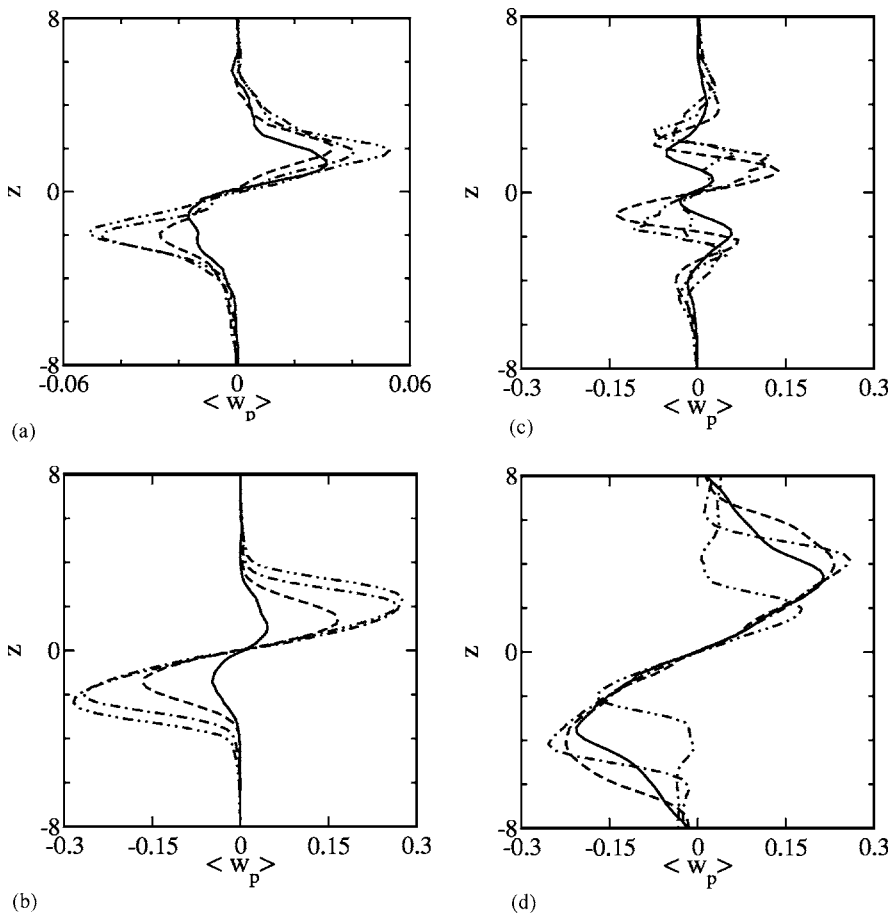


FIG. 12. Mean vertical velocity profiles for the particle phase at: (a)  $t = 24$ , (b)  $t = 48$ , (c)  $t = 72$ , and (d)  $t = 96$ . Legend: (—)  $St=0.3$ ; (- - -)  $St=0.6$ ; (· · ·)  $St=1$ ; (- · - ·)  $St=2$ .

In contrast to the fluid flow, the particle phase has a nonzero plane-averaged vertical velocity. The variation in time of this mean vertical velocity for different Stokes numbers is presented in Fig. 12. Locally, the velocity grows fast initially and reaches significant values at  $t=48$ . At  $t=72$ , when pairing is initiated, the velocity at the edge of the mixing layer changes sign and starts driving the particles back to the center (in accordance with Fig. 10). Once the pairing process is over, the mean vertical velocity again regains a shape similar to the initial one (at  $t=96$ ). From an Eulerian modeling standpoint, the nonzero mean vertical velocity is a key controlling quantity; for example, in particle-laden turbulent pipe flows where particles have a nonzero mean wallward velocity due to turbophoresis.<sup>39</sup> The role of this convective transport is analyzed further in the next section. To the best of our knowledge, these statistics have not been presented before for a two-dimensional mixing layer.

### C. Mean momentum balance for the particle phase

The plane-averaged particle number density and momentum equations are obtained by performing a streamwise average over the *spanwise averaged* equations.<sup>38</sup> The following transport equations are then obtained:

$$\frac{\partial \langle n \rangle}{\partial t} + \frac{\partial}{\partial z} \langle n \rangle \langle w_p \rangle = 0, \quad (10)$$

$$\begin{aligned} \frac{\partial}{\partial t} \langle n \rangle \langle u_p \rangle &= - \frac{\partial}{\partial z} \langle n \rangle \langle w_p \rangle \langle u_p \rangle + \frac{1}{\rho_D} \langle n f_{x,DC} \rangle \\ &+ \frac{\partial}{\partial z} \langle n \rangle (\langle w_p \rangle \langle u_p \rangle - \langle u_p w_p \rangle), \end{aligned} \quad (11)$$

$$\begin{aligned} \frac{\partial}{\partial t} \langle n \rangle \langle w_p \rangle &= - \frac{\partial}{\partial z} \langle n \rangle \langle w_p \rangle \langle w_p \rangle + \frac{1}{\rho_D} \langle n f_{z,DC} \rangle \\ &+ \frac{\partial}{\partial z} \langle n \rangle (\langle w_p \rangle \langle w_p \rangle - \langle w_p w_p \rangle). \end{aligned} \quad (12)$$

The interesting points to note in these equations, in comparison to the averaged equations for the fluid flow [Eqs. (6) and (7)], are the absence of viscous diffusion and pressure gradient terms, and the nonzero convective term due to the finite mean vertical velocity. In addition, the particle phase is not incompressible, in the sense of the velocity field being divergence free; accumulation and depletion of particles correspond to compression and dilation of the velocity field.

For the fluid flow, the only agent driving changes in the mean streamwise velocity is the modal stress derivative term. A comparison of the particle modal stress averaged over the vertical direction is shown in Fig. 13. The particle phase shows a behavior similar to that of the fluid phase, except for a systematic lag, which is as much as ten nondimensional time units for  $St=2$ . This points to a history effect in the

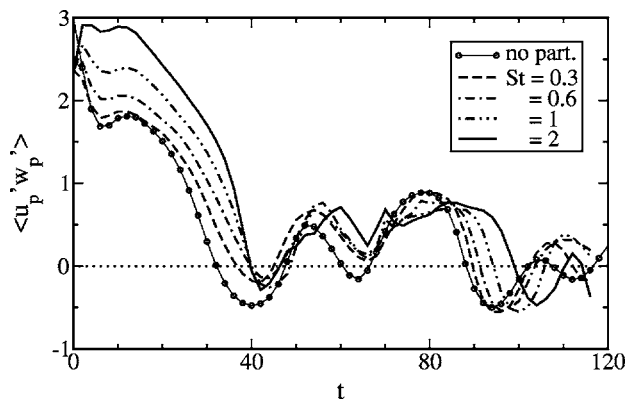


FIG. 13. Evolution of the particle-phase modal stress averaged over the mixing layer.

particle phase directly proportional to the Stokes number. The lower Stokes number particles are able to follow the flow dynamics with a fixed lag, but  $St=2$  particles are unable to follow the sign changes in the fluid average modal stress. This is because  $St=2$  particles are almost completely depleted from the mixing layer and therefore do not feel the changes in the fluid modal stress happening in the center of the layer.

The overall magnitude of the particle-phase modal stress remains of the same order as that of the flow. For the fluid, the mixing layer could be characterized as growing or

shrinking based on the sign of the averaged modal stress term. The same cannot be said for the particle phase, as other equally significant terms exist.

From the particle patterns presented before, it is obvious that the particle phase does not behave like a typical mixing layer, with the particle concentration being highly nonuniform. Analyzing the momentum balance should provide insight into the main particle transport processes. The streamwise momentum balances for particles with  $St=0.6$  and  $1$  are presented in Figs. 14 and 15, for two different times. The particle streamwise momentum balance is dominated by convection by the mean vertical velocity; the modal stress derivative and drag force terms are, however, never negligible. From the sign of the drag force, it can be concluded that the particles are driven by the flow (lag the flow) at least up to  $t=48$ . However, at  $t=24$ , there is a region in the center of the mixing layer where the particles lead the flow. This is due to the motion of particles from the core of the vortex towards the braid region where the mean velocity gradient is lower. For  $St=0.6$ , the convective term is smaller than the modal stress derivative term, whereas for  $St=1$  it is greater. This shows that the particle-phase modal stress is not as sensitive to the Stokes number as the mean vertical velocity.

The shape of the convective term (negative in the core and positive at the edge on the positive  $z$  side) reflects the depletion of streamwise momentum in the core and accumulation near the periphery of the vortices. The momentum

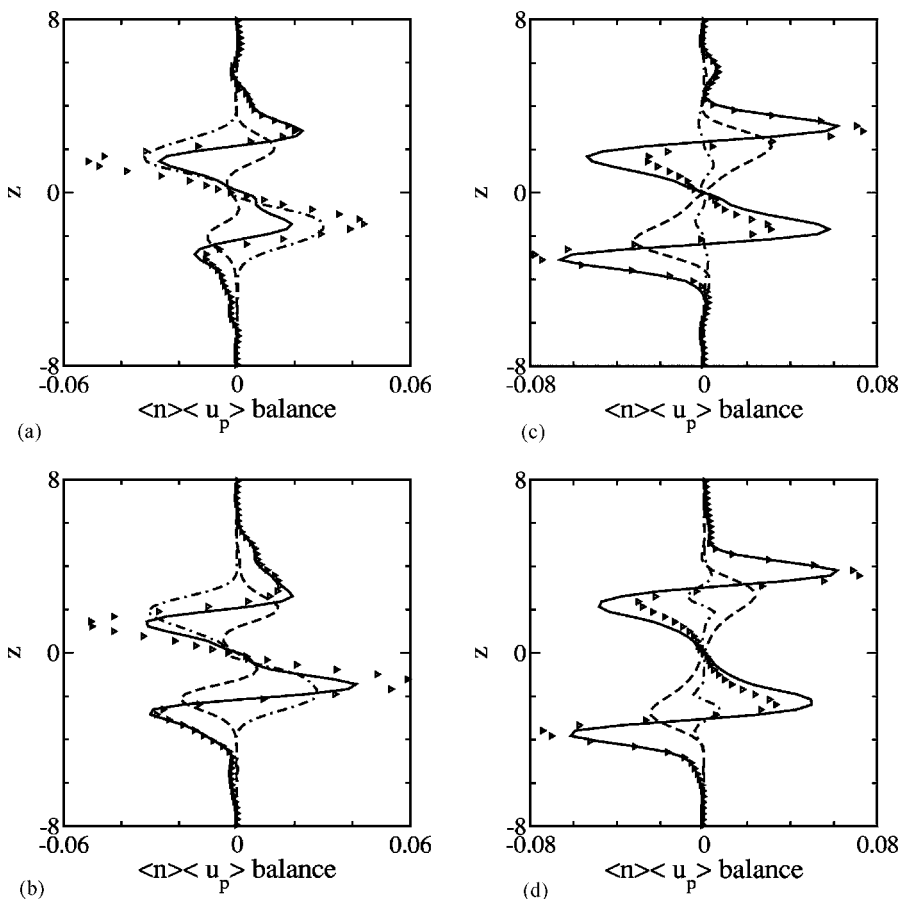


FIG. 14. Particle-phase streamwise momentum balance at  $t=24$  and  $48$ . Legend: (—) convective term; (---) drag force; (···) modal stress derivative term; (▷▷▷) sum of the RHS. (a)  $t=24, St=0.6$ ; (b)  $t=24, St=1$ ; (c)  $t=48, St=0.6$ ; (d)  $t=48, St=1$ .

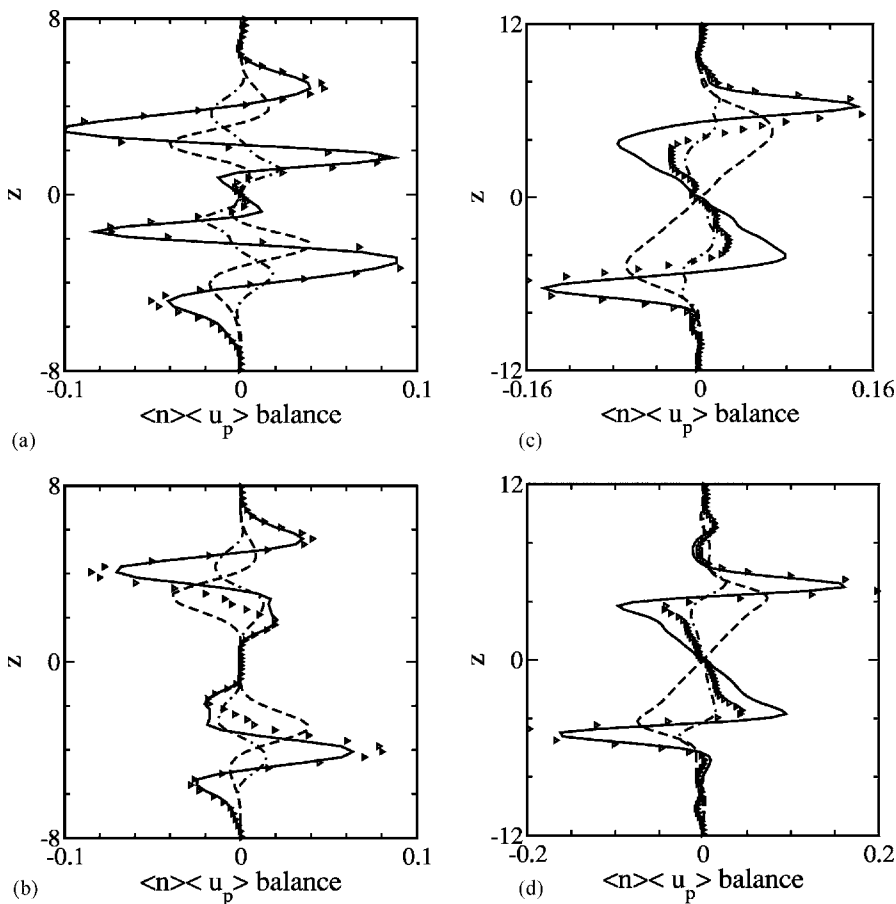


FIG. 15. Particle-phase streamwise momentum balance at  $t=72$  and  $96$ . Legend: (—) convective term; (---) drag force; (···) modal stress derivative term; ( $\triangleright\triangleleft$ ) sum of the RHS. (a)  $t=72$ ,  $St=0.6$ ; (b)  $t=72$ ,  $St=1$ ; (c)  $t=96$ ,  $St=0.6$ ; (d)  $t=96$ ,  $St=1$ .

balance for the particle phase cannot be directly compared to the particle-phase velocity plots presented before, because of the variation in the number density. Therefore, the convection term represents both, the change in momentum due to variations in the vertical mass flux ( $\langle n \rangle \langle w_p \rangle$ ), and due to the gradient in the streamwise velocity. A direct comparison for the growth of the velocity layers will require the particle equations to be rewritten in nonconservative form.

At  $t=48$ , the modal stress term for both the fluid flow and the particles is small (Fig. 13). Therefore, the particle streamwise momentum balance is governed only by the convection term and the drag force. Up to  $t=48$ , the drag force slows down the rate of spread of the particle streamwise momentum. Because the drag force is pulling the particles, it has the effect of increasing the particle streamwise momentum and therefore it acts against the growth of the particle layer. This simply means that particles arriving from lower velocity regions due to convection, get accelerated by the drag force.

The streamwise momentum balances at  $t=72$  and  $96$  (Fig. 15) reveal the increasing role of the convection term in transporting streamwise momentum laterally. The magnitude of the convective term increases continuously with time (note the change in the range of the abscissa), whereas the magnitudes of the other terms do not. In fact, Fig. 13 shows that the particle-phase modal stress follows the fluid phase values quite closely in magnitude and as a result ceases to play an important role in the lateral transport of streamwise momentum. The rate of change of particle streamwise mo-

mentum becomes almost equal to the convective term. At  $t=96$ , after the pairing process [Figs. 15(c) and 15(d)], the streamwise momentum balance takes a form similar to that at the early evolution of the mixing layer with the significant exception that the particle-phase modal stress term is much smaller than the other terms. The drag force increases in magnitude and remains significant in the overall balance. The mixing layer can be divided into two regions: the streamwise momentum depletion region and the accumulation region. In the depletion region the drag force acts against the convection term, and in the accumulation region, both act in tandem.

## V. CONCLUSIONS

Simulations of two-dimensional, particle-laden mixing layers were performed for particles with various Stokes numbers under the assumption of one-way coupling using the Eulerian-Lagrangian method. Transport of particles with four Stokes numbers, viz., 0.3, 0.6, 1, and 2, was analyzed. Most of the earlier studies on particle-laden mixing layers have focused on characterizing particle transport using Lagrangian dispersion indicators. In this work, analysis of two-phase momentum transfer was presented in the Eulerian frame of reference by looking at the balance of fluid-phase mean momentum, mean kinetic energy, modal kinetic energy, and particle-phase mean momentum.

The differences in the dominant mechanisms of vertical transport of streamwise momentum between the fluid and

particle phases was clearly brought out. In the fluid phase, the growth of the mixing layer was shown to be brought about by the energy transfer from the mean to the modes and the transport of mean momentum by the modes. The transport processes in the fluid phase were fully characterized by looking at the balances of the mean and modal kinetic energies.

The centrifuging effect of the spanwise Kelvin-Helmholtz vortices as a function of particle Stokes number was discussed. It was shown that in contrast to the fluid phase, the particle phase has a nonzero mean vertical velocity due to the centrifuging effect. The particle-phase modal stress was shown to remain strongly correlated to the fluid-phase modal stress throughout the simulation period. However, a systematic lag is seen to exist between their evolution with the lag being higher for higher Stokes numbers.

It was shown that the convection of streamwise momentum by the plane-averaged particle-phase vertical velocity is the dominant term in the particle streamwise momentum balance. The mean particle vertical velocity assumes significant values depending on the value of the particle Stokes numbers. Together with the gradient in the streamwise velocity along the vertical direction, the convection term gains in importance. Thus the vertical drag force indirectly plays a more significant role in the streamwise particle momentum balance than the streamwise drag force. Except at the pre-pairing stage and during pairing, particle velocity lags the fluid velocity, because of the motion of particles from low-velocity regions to high-velocity regions. During pairing, particles from the free stream are engulfed into the mixing layer and they can transfer energy to the fluid (under two-way coupling).

Although the drag force and the particle-phase modal stress play an important role in the evolution of the particle-phase mixing layer in the early stages, their role was shown to decrease during the pairing process. After pairing, the particle-phase mean streamwise momentum balance is accounted for by the convection and drag force terms. The particle-phase modal stress term becomes less significant as its magnitude remains strongly connected to the fluid phase modal stress. The effect of particle transport on the fluid flow will be presented in Part II of this study.

## ACKNOWLEDGMENTS

The authors would like to thank Professor Yadigaroglu for his support and guidance. C.N. would like to thank the European Research Community on Flow Turbulence and Combustion (ERCOFTAC) for funding this research.

<sup>1</sup>J. K. Eaton and J. R. Fessler, "Preferential concentration of particles by turbulence," *Int. J. Multiphase Flow* **20**, 169 (1994).

<sup>2</sup>S. Elghobashi, "On predicting particle-laden turbulent flows," *Appl. Sci. Res.* **52**, 309 (1994).

<sup>3</sup>C.-M. Ho and P. Huerre, "Perturbed free shear layers," *Annu. Rev. Fluid Mech.* **16**, 365 (1984).

<sup>4</sup>G. M. Corcos and F. S. Sherman, "The mixing layer: Deterministic models of a turbulent flow. Part 1. Introduction and the two-dimensional flow," *J. Fluid Mech.* **139**, 29 (1984).

<sup>5</sup>S. J. Lin and G. M. Corcos, "The mixing layer: deterministic models of a turbulent flow. Part 3. The effect of plane strain on the dynamics of streamwise vortices," *J. Fluid Mech.* **141**, 139 (1984).

<sup>6</sup>G. L. Brown and A. Roshko, "On density and large structure in turbulent mixing layers," *J. Fluid Mech.* **64**, 775 (1974).

<sup>7</sup>P. Huerre and P. A. Monkewitz, "Absolute and convective instabilities in free shear layers," *J. Fluid Mech.* **159**, 151 (1985).

<sup>8</sup>A. A. Dimas and K. T. Kiger, "Linear instability of a particle-laden mixing layer with a dynamic dispersed phase," *Phys. Fluids* **10**, 2539 (1998).

<sup>9</sup>C. Narayanan and D. Lakehal, "Temporal instabilities of a mixing layer with uniform and nonuniform particle loadings," *Phys. Fluids* **14**, 3775 (2002).

<sup>10</sup>R. T. Pierrehumbert and S. E. Widnahl, "The two- and three-dimensional instabilities of a spatially periodic shear layer," *J. Fluid Mech.* **114**, 59 (1982).

<sup>11</sup>A. B. Cortesi, G. Yadigaroglu, and S. Banerjee, "Numerical investigation of the formation of three-dimensional structures in stably-stratified mixing layers," *Phys. Fluids* **10**, 1449 (1998).

<sup>12</sup>L. P. Bernal and A. Roshko, "Streamwise vortex structure in plane mixing layers," *J. Fluid Mech.* **170**, 499 (1986).

<sup>13</sup>B. J. Lazaro and J. C. Lasheras, "Particle dispersion in a turbulent, plane, free shear layer," *Phys. Fluids A* **1**, 1035 (1989).

<sup>14</sup>B. J. Lazaro and J. C. Lasheras, "Particle dispersion in the developing free shear layer. part 1. unforced flow," *J. Fluid Mech.* **235**, 143 (1992).

<sup>15</sup>B. J. Lazaro and J. C. Lasheras, "Particle dispersion in the developing free shear layer. Part 2. Forced flow," *J. Fluid Mech.* **235**, 179 (1992).

<sup>16</sup>K. T. Kiger and J. C. Lasheras, "The effect of vortex pairing on particle dispersion and kinetic energy transfer in a two-phase turbulent shear layer," *J. Fluid Mech.* **302**, 149 (1995).

<sup>17</sup>K. T. Kiger and J. C. Lasheras, "Dissipation due to particle/turbulence interaction in a two-phase, turbulent, shear layer," *Phys. Fluids* **9**, 3005 (1997).

<sup>18</sup>K. Hishida, A. Ando, and M. Maeda, "Experiments on particle dispersion in a turbulent mixing layer," *Int. J. Multiphase Flow* **18**, 181 (1992).

<sup>19</sup>F. Wen, N. Kamalu, J. N. Chung, C. T. Crowe, and T. R. Troutt, "Particle dispersion by vortex structures in plane mixing layers," *J. Fluids Eng.* **114**, 657 (1992).

<sup>20</sup>R. Chein and J. N. Chung, "Effects of vortex pairing on particle dispersion in turbulent shear flows," *Int. J. Multiphase Flow* **13**, 785 (1987).

<sup>21</sup>J. E. Martin and E. Meiburg, "The accumulation and dispersion of heavy particles in forced two-dimensional mixing layers. I. The fundamental and subharmonic cases," *Phys. Fluids* **6**, 1116 (1994).

<sup>22</sup>N. Raju and E. Meiburg, "The accumulation and dispersion of heavy particles in forced two-dimensional mixing layers. Part 2: The effect of gravity," *Phys. Fluids* **7**, 1241 (1995).

<sup>23</sup>B. Marcu and E. Meiburg, "The effect of streamwise braid vortices on the particle dispersion in a plane mixing layer. I. Equilibrium points and their stability," *Phys. Fluids* **8**, 715 (1996).

<sup>24</sup>B. Marcu, E. Meiburg, and N. Raju, "The effect of streamwise braid vortices on the particle dispersion in a plane mixing layer. I. Nonlinear particle dynamics," *Phys. Fluids* **8**, 734 (1996).

<sup>25</sup>B. Marcu and E. Meiburg, "Three dimensional features of particle dispersion in a nominally plane mixing layer," *Phys. Fluids* **8**, 2266 (1996).

<sup>26</sup>W. Ling, J. N. Chung, T. R. Troutt, and C. T. Crowe, "Direct numerical simulation of a three-dimensional mixing layer with particle dispersion," *J. Fluid Mech.* **358**, 61 (1998).

<sup>27</sup>S. K. Aggarwal, J. B. Yapo, F. F. Grinstein, and K. Kailasanath, "Numerical simulation of particle transport in planar shear layers," *Comput. Fluids* **25**, 39 (1996).

<sup>28</sup>Z. Hu, X. Luo, and K. H. Luo, "Numerical simulation of particle dispersion in a spatially developing mixing layer," *Theor. Comput. Fluid Dyn.* **15**, 403 (2002).

<sup>29</sup>Q. Wang, K. D. Squires, and L.-P. Wang, "On the effect of nonuniform seeding on particle dispersion in two-dimensional mixing layers," *Phys. Fluids* **10**, 1700 (1998).

<sup>30</sup>M. C. Soteriou and X. Yang, "Particle dispersion in variable density and viscosity shear flows," *Phys. Fluids* **11**, 1373 (1999).

<sup>31</sup>X. Yang, N. H. Thomas, and L. J. Guo, "Particle dispersion in organized vortex structures within turbulent free shear flow," *Chem. Eng. Sci.* **55**, 1305 (2000).

<sup>32</sup>C. Narayanan, D. Lakehal, and G. Yadigaroglu, "Linear stability analysis of particle-laden mixing layers using lagrangian particle tracking," *Powder Technol.* **125**, 122 (2002).

<sup>33</sup>M. R. Maxey and J. K. Riley, "Equation of motion for a small rigid sphere in a nonuniform flow," *Phys. Fluids* **26**, 883 (1983).

<sup>34</sup>X.-L. Tong and L.-P. Wang, "Two-way coupled particle-laden mixing layer. Part 1: Linear instability," *Int. J. Multiphase Flow* **25**, 575 (1999).

- <sup>35</sup>G. P. Klaassen and W. R. Peltier, "The evolution of finite amplitude Kelvin-Helmholtz billows in two spatial dimensions," *J. Atmos. Sci.* **42**, 1321 (1985).
- <sup>36</sup>D. Oster and I. J. Wignanski, "The forced mixing layer between parallel streams," *J. Fluid Mech.* **123**, 91 (1982).
- <sup>37</sup>K. D. Squires and J. K. Eaton, "Particle response and turbulence modification in isotropic turbulence," *Phys. Fluids A* **2**, 1191 (1990).
- <sup>38</sup>D. Lakehal and C. Narayanan, "Numerical analysis of the continuum formulation for the initial evolution of mixing layers with particles," *Int. J. Multiphase Flow* **29**, 927 (2003).
- <sup>39</sup>J. Young and A. Leeming, "A theory of particle deposition in turbulent pipe flow," *J. Fluid Mech.* **340**, 129 (1997).